ELSEVIER

Journal of Nuclear Materials 266–269 (1999) 1240–1246

journal of nuclear materials

Radial current and flows in the scrape-off layer of a tokamak

M. Van Schoor *, R. Weynants

Laboratorium voor Plasmafysica/Laboratoire de Physique des Plasmas, Association Euratom-Belgian State, Trilateral Euregio Cluster, Koninklijke Militaire School/Ecole Royale Militaire, Renaissancelaan 30, 1000 Brussels, Belgium

Abstract

A simple one-dimensional, isothermal model is presented to study the flow fields and the radial current in the scrape-off layer of a tokamak. It is shown how, using basic tensor properties, the radial current can be expressed as a function of the flows and the radial electric field in a very simple way, provided that none of the curvature terms are neglected in the toroidal momentum equation. The flows are computed by solving the parallel momentum equation together with the continuity equation. We have included convection, viscosity and neutral drag in all the equations. This finally results in an almost linear relation between the radial electric field and the radial current as is experimentally observed. Two types of boundary conditions at the limiter or target, applied at the magnetic pre-sheath or the material boundary, in the past a source of contradiction, are studied in detail. We show that the viscosity in the parallel momentum equation levels out the marked difference which was encounterd in earlier theories between the two types of boundary conditions. Our model predicts the experimentally observed trends on TdeV, the only anomalous effect introduced being the diffusive radial velocity. The neutral interaction driven current is shown to be potentially very important. The physical content of the equations, their relation to the Bohm–Chodura criterion and the poloidal dependence of the currents are a point of particular attention.

Keywords: Tokamak de Varennes; Radial electric field

1. Introduction

The aim of this paper is to study the radial current, the flows and the pressure in the scrape-off layer of a Tokamak as a function of an applied radial electric field. Such a study addresses the mechanisms that govern non-ambipolar radial transport and plasma conductivity which can be important in H-mode bifurcation studies [1,2] or biasing experiments [3]. Recently, Chankin and Stangeby [4] showed the importance of the toroidicity and of the boundary conditions on the net radial conductivity. Their model however fails to predict the correct relation between the applied field and the current as observed in the TdeV biasing experiment [5]. Earlier the effect of anomalous inertia and anomalous viscosity was analysed by Rozhansky and Tendler [6]. Both studies however neglect the influence of neutrals.

In Ref. [7] we have built a more complete classical model including neutral drag and viscosity, while at the same time taking care to correctly implement all the geometrical toroidicity effects. We now wish to further analyse the radial current, estimating the influence of the curvature of the geometry, while also studying the poloidal dependence of the current density.

The scrape-off layer of a divertor or limiter tokamak can be studied using an isothermal, collisional fluid approximation [8,9]. The steady state continuity and total momentum equations read

$$\overline{\nabla} \cdot (n\bar{V}) = 0, \tag{1}$$

$$\overline{\nabla} \cdot (m \cdot n \cdot \overline{V}\ \overline{V}) = -\overline{\nabla}_p - \overline{\nabla} \cdot \bar{\bar{\pi}} + (\bar{J} \times \bar{B}) + \bar{F}_{\text{neutrals}}, \tag{2}$$

where $\bar{V}$ is the flow velocity, n the density, p the total pressure, $\bar{\bar{\pi}}$ the viscosity tensor, J the current density, m the ion mass, B the magnetic field and the neutral drag force is given by

$$\bar{F}_{\text{neutrals}} = -\nu \cdot \bar{V}, \tag{3}$$

* Corresponding author. E-mail: vanschoor@fusion.rma.ac.be

0022-3115/99/$ – see front matter
PII: S0022-3115(98)00893-9

where v is a drag coefficient yet to be defined. These equations will be used to compute the radial current, the density (or the pressure) and the flow parallel to the magnetic field $V_{//}$.

The toroidal projection of the momentum Eq. (2) will be used in Section 3 to compute the surface averaged radial current. The unknown flow velocity and the density appearing in the equation for the current, will be found in Section 4 by solving the continuity equation together with the parallel projection of the total momentum equation. In Section 5, results of the numerical model are shown and compared with the experimental findings.

2. Basic definitions and properties

If we consider the toroidal component of the total momentum Eq. (2), the radial current is expressed as

$$I_r = \left\langle\left\langle \frac{1}{B_2}(\overline{\nabla}\cdot(mn\overline{V}\ \overline{V})_3 \right\rangle\right\rangle + \left\langle\left\langle \frac{1}{B_2}(\overline{\nabla}\cdot\bar{\bar{\pi}})_3 \right\rangle\right\rangle - \left\langle\left\langle \frac{1}{B_2}F_{\text{neutrals}} \right\rangle\right\rangle, \tag{4}$$

where the double brackets denote the integral over the magnetic surface through which the current flows and (1,2,3) are curvilinear co-ordinates in the radial poloidal and toroidal direction of the machine. The pressure term has disappeared due to axi-symmetry.

It is easy to show that the two tensorial quantities in this equation

$$\left\langle\left\langle \frac{(\overline{\nabla}\cdot\bar{\bar{\mathbf{T}}})_3}{B_2} \right\rangle\right\rangle = 2\pi\int_{x_2}\frac{\left(\overline{\nabla}\cdot\bar{\bar{\mathbf{T}}}\right)_3}{B_2}\cdot h_2\cdot h_3\cdot \mathrm{d}x_2, \tag{5}$$

where $\bar{\bar{\mathbf{T}}}$ is the convection or viscosity tensor and the h_i are the metric coefficients of the curvilinear system of reference, can be written as the sum of the following terms:

$$(\mathrm{I}) = \frac{2\pi}{B_o\cdot R_o\tilde{\Theta}}\frac{\partial}{\partial x_1}\int_{x_2}(h_2\cdot h_3^2\cdot T_{1,3})\cdot \mathrm{d}x_2, \tag{6}$$

$$(\mathrm{II}) = \frac{2\pi}{B_o\cdot R_o\tilde{\Theta}}\cdot[h_1\cdot h_3^2\cdot T_{2,3}]\big|_{x_2}. \tag{7}$$

Note that this is only possible when no curvature terms are neglected and that the expression is valid for a general cross-section. We only suppose that the tensors are symmetric. In the rest of the text however we will use a circular cross-section and neglect the Shafranov shift so that $h_1 = 1$, $h_2 = r$ (minor radius) and $h_3 = R$ (major radius). Fig. 1 depicts a cross-section of the machine and the system of reference we use. We suppose that there are two material plates in the scrape-off layer, modelling a limiter or a divertor.

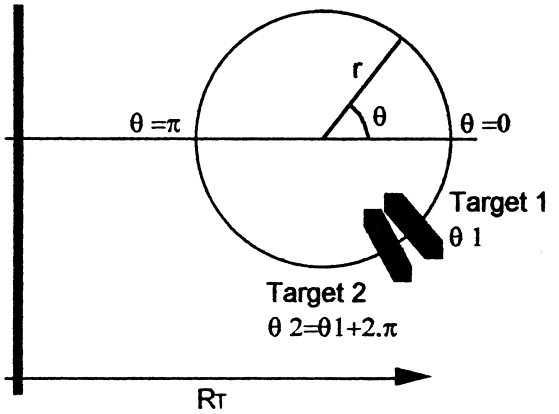

Fig. 1. Poloidal cross-section and co-ordinate system.

The type (I) current involves the computation of element (1,3) of the considered tensor. Therefore, it introduces the radial velocity in the model via the convection tensor. This is important as we will consider the radial velocity to be of turbulent origin and so introduce the only anomalous effect in our model via this current. Element (1,3) of the parallel or bulk viscosity is zero. As a consequence this viscosity has no type (I) contribution.

The shear and perpendicular viscosity tensors each have non-zero elements (1,3) and (2,3). Their contributions in the current were checked and can be shown to be negligible [7].

In the scrape-off layer the magnetic field interesects material boundaries. The magnetic surfaces are open and the partial integration term (II) is not zero. It therefore introduces the boundary conditions in the model.

3. The radial current

Using the property (Eqs. (6) and (7)) discussed in the Section 2, we can evaluate the different terms in Eq. (4). We will suppose that all the variables are only function of θ (except M_E considered constant and imposed by the applied bias) and introduce the following dimensionless quantities:

$$\begin{aligned} &V_{//} = M\cdot C_s, \qquad V_\perp = \xi\cdot M_E\cdot C_s\cdot\Theta,\\ &V_\theta = \sin\alpha\cdot C_s\cdot(M+\xi\cdot M_E) = \sin\alpha\cdot C_s\cdot M_p,\\ &\xi = R/R_o; \quad \varepsilon = r/R_o; \quad C_s = \sqrt{\frac{T_i+T_e}{m_i}}. \end{aligned} \tag{8}$$

α is the angle between parallel and toroidal direction and Θ is the magnetic pitch. We can then compute the different contributions in the radial current.

(i) *for the neutral drag*:

$$\mathrm{I}_{\mathrm{r},n} = \frac{2\pi\varepsilon\cos\,\alpha\cdot R_{\mathrm{o}}^2 C_{\mathrm{s}}}{\Theta B_{\mathrm{o}}}\left[\left\{\int_{\theta=\theta_1}^{\theta_2}\xi^2\cdot v\cdot M\cdot \mathrm{d}\theta\right\} - M_{\mathrm{E}}\Theta^2\cdot\left\{\int_{\theta=\theta_1}^{\theta_2}\xi^3\cdot v\,\mathrm{d}\theta\right\}\right]. \tag{9}$$

(ii) *for the convection tensor*:

Here we have to distinguish between a type (I) and a type (II) contributions. For (I) we find

$$\begin{aligned}(\mathrm{I}) &= I_{\mathrm{r,\ Conv(I)}}\\ &= \frac{2\pi m\cdot D.\cos\,\alpha\cdot \mathrm{C_s}}{\mathrm{B_o}\cdot \mathrm{R_o}\lambda_{\mathrm{r}}\Theta}\cdot\left[\left\{\frac{\partial}{\partial r}r\cdot\int_{\theta=\theta_1}^{\theta_2}(R^2 n\cdot M)\cdot \mathrm{d}\theta\right\}\right.\\ &\quad -\left\{\Theta^2\frac{\partial}{\partial r}r\cdot\int_{\theta=\theta_1}^{\theta_2}(R^2 n\cdot\xi)\cdot \mathrm{d}\theta\right\}\cdot M_{\mathrm{E}}\\ &\quad \left.-\left\{\Theta^2\cdot r\cdot\int_{\theta=\theta_1}^{\theta_2}(R^2 n\cdot\xi)\cdot \mathrm{d}\theta\right\}\left(\frac{\partial}{\partial r}M_{\mathrm{E}}\right)\right].\end{aligned} \tag{10}$$

This current proves to be very small in comparison to the other contributions.

The type (II) current is given by

$$\begin{aligned}(\mathrm{II}) &= I_{\mathrm{r,\ Conv(II)}}\\ &= \frac{2\pi}{B_o R_{\mathrm{o}}}\cos^2\,\alpha C_{\mathrm{s}}^2\left[n(M+\xi M_{\mathrm{E}})\cdot(M-\Theta^2\xi M_{\mathrm{E}})\right]_{\theta_1}^{\theta_2}\end{aligned} \tag{11}$$

and the radial velocity is modelled as anomalous diffusion:

$$n = n_{\mathrm{o}}(\theta)\cdot \mathrm{e}^{-(r/\lambda_r)},\qquad V_{\mathrm{r}} = -\frac{D}{n}\frac{\partial n}{\partial r} = \frac{D}{\lambda_r}. \tag{12}$$

The type (II) terms are partial integration terms, introducing the effect of the material boundaries. We therefore must decide where exactly the boundary should be taken. A first possibility is to evaluate the quantities at the entrance of the magnetic pre-sheath (s), resulting in

$$\begin{aligned}I^{(\mathrm{s})}_{\mathrm{r,\ Conv(II)}} &= \frac{2\pi}{B_{\mathrm{o}}}\cdot\frac{R_T^2}{R_{\mathrm{o}}}\cdot m\cdot\cos^2\,\alpha\cdot C_{\mathrm{s}}^2\\ &\quad\cdot\left[(n_{\mathrm{s}2}-n_{\mathrm{s}1}) - M_{\mathrm{E}}\cdot\xi_T(1+\Theta^2)\cdot(n_{\mathrm{s}2}+n_{\mathrm{s}1})\right],\end{aligned} \tag{13}$$

R_T being the major radius at which the limiter is located. In Ref. [4], on the other hand, it is argued that one should rather consider the quantities at the material boundary. It is possible to relate the values of n and M at the entrance of the magnetic pre-sheath to those at the plate (p) using a simplified version of the parallel momentum equation:

$$(\overline{\nabla}\cdot(m\cdot n\cdot\overline{V}\ \overline{V}))_{//} = -(\overline{\nabla}P)_{//}, \tag{14}$$

where the parallel viscosity is neglected because the sheath is collisionless.This results in

$$\begin{aligned}I^{(\mathrm{p})}_{\mathrm{r,\ Conv(II)}} &= \frac{2\pi}{B_{\mathrm{o}}}\cdot\frac{R_T^2}{R_{\mathrm{o}}}\cdot m\cdot\cos^2\,\alpha\\ &\quad\cdot C_{\mathrm{s}}^2\left[2(n_{\mathrm{s}2}-n_{\mathrm{s}1}) - M_{\mathrm{E}}\cdot\xi_T\cdot(n_{\mathrm{s}2}+n_{\mathrm{s}1})\right]\end{aligned} \tag{15}$$

(iii) *for the parallel viscosity tensor*:

Element (1,3) of this tensor is zero, resulting in only a type (II) contribution. As the sheath is considered collisionless, we only consider the (s) type boundary condition for this current contribution and find accordingly

$$I^{(\mathrm{s})}_{\mathrm{r,Vis}} = -\frac{4\pi}{B_{\mathrm{o}}}\left[\frac{R_T}{R_{\mathrm{o}}}\right]^2\frac{C_{\mathrm{s}}\cdot\sin\,\alpha\cdot\cos^2\,\alpha}{\varepsilon}\eta_0\cdot([M'_{\mathrm{s}2}-M'_{\mathrm{s}1}]), \tag{16}$$

in which $\eta_0 = 0.96nT_i\tau_i$ is the viscosity coefficient and τ_i the ion collision time.

The total radial current then is given by the sum of Eqs. (9) and (13) or Eqs. (15) and (16):

$$I_{\mathrm{r}} = I_{\mathrm{r},n} + I^{(\mathrm{s})\mathrm{or}(\mathrm{p})}_{\mathrm{r,\ Conv(II)}} + I_{\mathrm{r,\ Vis}}. \tag{17}$$

4. The parallel momentum and continuity equations

The current cannot be evaluated without the knowledge of M and n as functions of θ. These profiles are obtained by solving the continuity and the parallel momentum equations, which read

$$n' = \frac{Fn - n(M'+\xi'\cdot M_{\mathrm{E}}) - n\frac{\xi'}{\xi}M_{\mathrm{p}}}{M_{\mathrm{p}}}, \tag{18}$$

$$\begin{aligned}&M''\cdot\left\{-\frac{4}{3}A\cdot M_{\mathrm{p}}\right\} + M'\cdot\left\{n\cdot M_{\mathrm{p}}^2 - n - 2\cdot A\cdot\frac{\xi'}{\xi}\cdot M_{\mathrm{p}}\right\}\\ &\quad+\left\{F\cdot[n+M\cdot n\cdot M_{\mathrm{p}}] + n\cdot M_{\mathrm{E}}\cdot\xi'\cdot(M-\Theta^2\xi M_{\mathrm{E}})\right.\\ &\quad\cdot M_{\mathrm{p}} + A\frac{(\xi')^2}{\xi}\cdot M_{\mathrm{E}}\cdot M_{\mathrm{p}} - n\frac{\xi'}{\xi}\cdot M_{\mathrm{p}}\\ &\quad\left.-\xi'\cdot n\cdot M_{\mathrm{E}} + A\cdot\frac{2}{3}\cdot\xi''\cdot M_{\mathrm{E}}\cdot M_{\mathrm{p}} + n\cdot B\cdot MM_{\mathrm{p}}\right\} = 0\end{aligned} \tag{19}$$

with

$$F = \frac{r\cdot D}{\lambda_r^2\cdot\sin\,\alpha\cdot C_{\mathrm{s}}},\quad A = \frac{\eta_0\cdot\sin\,\alpha}{m\cdot r\cdot C_{\mathrm{s}}},\quad B = \frac{v^*\cdot\varepsilon\cdot R_{\mathrm{o}}}{C_{\mathrm{s}}\cdot m\cdot\sin\,\alpha}.$$

The boundary conditions available for these equations are given by the Bohm–Chodura criterion [10], which in our variables reads

$$M + \xi_T \cdot M_E = \pm 1. \tag{20}$$

5. Results and discussion

The system of Eqs. (18) and (19) describes the evolution of the Mach number and of the density in the poloidal direction. Provided M_E is given, these equations can be integrated in the scrape-off layer from one target or limiter side, following the considered magnetic surface until the other target or limiter side is reached. This results in a set of density and Mach profiles. Then the current can be computed from Eq. (17), so that a plot of the current versus M_E can be made.

For a convenient comparison, the current will be represented in the dimensionless form introduced by Chankin and Stangeby [4] and defined as

$$I^* = \frac{I_r}{2\pi R_o} \frac{1}{e\langle n\rangle \rho C_s}; \quad \rho = \frac{C_s}{\omega_{io}} = \frac{m \cdot C_s}{e \cdot B_o}. \tag{21}$$

This definition makes the current independent of $\langle n\rangle$, the surface averaged density, and of the temperature so that comparison between different machines becomes possible. As we will introduce viscosity and neutral drag we need nevertheless the ion temperature, to compute the viscosity coefficient and the neutral density profile, both of which are machine dependent. Our reference case is the TEXTOR-94 L-mode edge plasma with $B_o = 2T$, $R_o = 1.75\,\mathrm{m}$ and $\varepsilon = 0.27$, for which the profiles were computed with *B*2, a two-dimensional plasma edge code, supplemented with EIRENE, a Monte–Carlo neutral particle code [9]. The used profiles are represented in Fig. 2. The limiter is considered at 45° below the equatorial plane at the outboard side, resulting in $\theta_1 = -\pi/4$ and $\theta_2 = \theta_1 + 2\pi$.

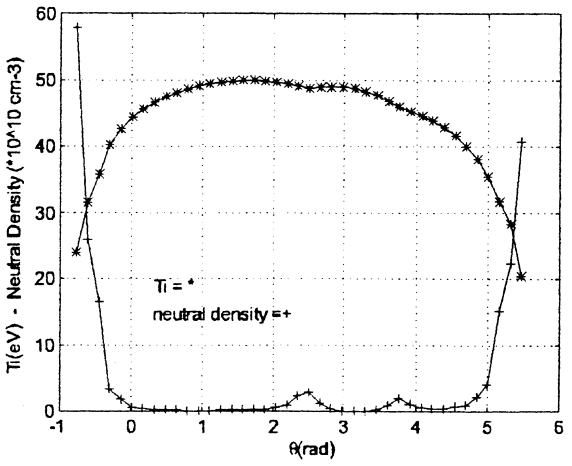

Fig. 2. Neutral density ($10^{10}\mathrm{cm}^{-3}$) and ion temperature (eV) as a function of poloidal angle.

We will start our discussion leaving the neutral interactions and the viscosity out of the parallel momentum equation (case $A = B = 0$). Next we include the neutral interactions and the viscosity and compare the full model with experimental measurements.

5.1. Case $A = 0$; $B = 0$

Eq. (19) then reduces to

$$M' = \{F \cdot [1 + M \cdot M_p] + M_E \cdot \xi' \cdot (M - \Theta^2 \xi M_E) \cdot M_p - \frac{\xi'}{\xi} \cdot M_p - \xi' \cdot M_E\} / \{1 - M_p^2\}, \tag{22}$$

while the density can be computed from

$$n' = -n \cdot \{F \cdot M + M' \cdot M_p + M_E \cdot \xi' \cdot (M - \Theta^2 \xi M_E)\}. \tag{23}$$

These are, to order of Θ^2, the equations as given by Chankin and Stangeby [4].

Eqs. (22) and (23) can be solved by imposing the boundary condition at one side of the domain and then to adjust F, which governs the steepness of the Mach profile, until also at the other side the correct boundary condition is reached.

F is found to vary with an average value of 0.25 when we vary M_E. As the density decay length in TEXTOR in the considered region is of the order of 3 cm, this value corresponds to $D = 1.8\ \mathrm{m}^2\ \mathrm{s}$, which is quite realistic. The solution of these equations, the resulting currents and a comparison with earlier theories by Chankin and Stangeby [4] and Rozhansky and Tendler [6] were extensively studied in Ref. [7].

Here, we wish to further analyse the equations. Eq. (22) is interesting because it introduces the Bohm–Chodura criterion in a natural way. Indeed, in the vicinity of the sheath, the temperature drops, the viscosity accordingly is reduced and Eqs. (19) and (22) become equivalent. Eq. (22) becomes singular when $M_p^2 = 1$, which means that the sheath is reached. We therefore find the same criterion as Chodura in [10].

The different terms in Eq. (22) can be interpreted in the following way. In the numerator:

(i) $F(1 + MM_p)$ is introduced by adding the continuity equation to the parallel momentum equation and describes the particle input in a flux tube. It is this term that governs the steepness of the Mach profile [4,7].

(ii) $M_E \cdot \xi' \cdot (M - \Theta^2 \xi M_E) \cdot M_p$ is introduced via the curvatre terms in the connnection error.

(iii) $\xi'/\xi \cdot M_p$ describes the variation of the cross-section of the flux tube when going from the outboard to the inboard side of the torus.

(iv) $\xi' \cdot M_E$ appears because we consider the parallel momentum equation, describing the transport of

parallel momentum. The convection tensor however describes the convection of this parallel momentum in the poloidal direction.

In the denominator the factor $(1 - M_p^2)$ appears. It is for this same reason as mentioned in (iv) that we do not find $(1 - M^2)$, but rather a function of the poloidal Mach number. Therefore, this phenomena is at the basis of the Bohm–Chodura criterion.

The term described in (iii) would place the eventual sonic transition, possible when solving Eq. (19), in the troath section of the flux tube, which is at the inboard side of the torus, in the equatorial plane where $\theta = \pi$. Due to the extra terms we see that the spot where the transition occurs is shifted. This is clearly depicted in Fig. 3, showing a solution where $M_E = 0.8$ and $F = 0.2295$. M_p increases to 1 and then decreases again. This means that the value chosen for F is too small. Indeed at the second target we see that $M_p < 1$ so that the Bohm–Chodura criterion is not met. The point where Mp reaches 1 however and where the transition occurs when we increase F is at $\theta = 3.8$ rad.

5.2. Case $A \neq 0$; $B \neq 0$

Eq. (19) is now a second order equation. F is not a free parameter and is taken equal to the average of the values necessary to fulfil the boundary conditions in Section 5.1. On both sides of the integration domain the Bohm–Chodura boundary conditions ($M_p = \pm 1$) are imposed. Solving the equations results in the plots represented in Fig. 4 for the Mach and density profiles and Fig. 5 for the meaningful current contributions.

We note the following:

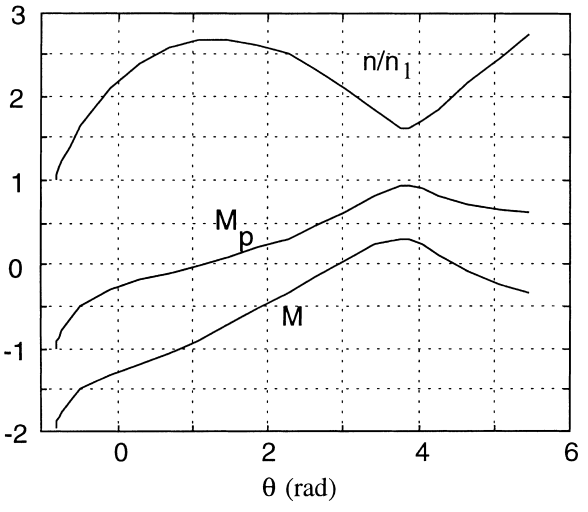

Fig. 3. n, M_p and M as functions of the poloidal angle for $M_E = 0.8$ and $F = 0.2295$.

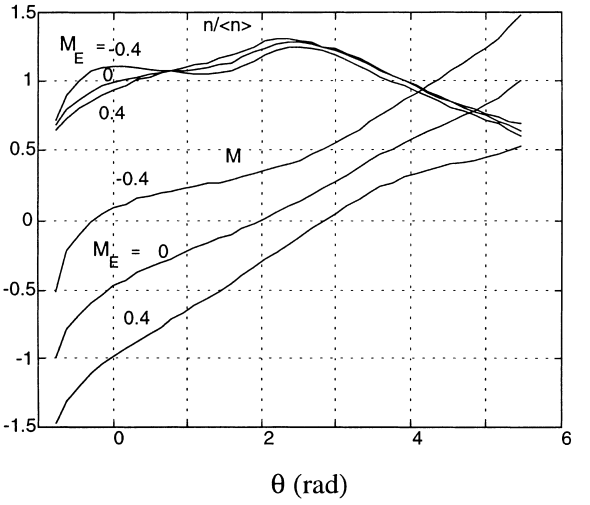

Fig. 4. Case $B \neq 0$, $A \neq 0$. Mach profiles (lower curves) and normalised density (upper curves) as functions of the poloidal angle for three cases of M_E.

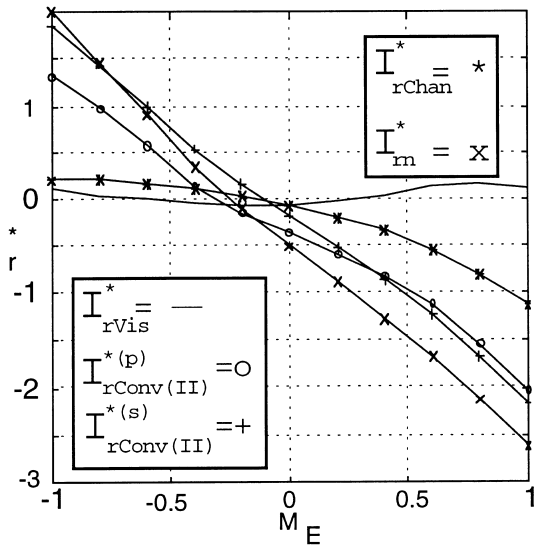

Fig. 5. Case $B \neq 0$, $A \neq 0$. Dimensionless currents as functions of M_E.

(i) $I^*_{r,\mathrm{Vis}}$ is small. As it is a type (II) current, it only depends on the values of the parameters at the level of the material boundary, where the temperature is much lower than average. This reduces the viscosity coefficient, proportional to $T_i^{5/2}$, and accordingly the current. It should also be noted that we took for the temperature profile a case without bias. It is clear that if the bias would have an influence on the temperature profile, possible asymmetries between the boundaries would have an influence on the current. Finally, we see that

$I^*_{\mathrm{r,\,Vis}}$ has no term proportional with M_{E}. This is due to our hypothesis that M_{E} is constant in the poloidal direction so that it disappears in Eq. (16). The result is that $I^*_{\mathrm{r,\,Vis}}$ is more or less constant over the whole region of values of M_{E}.

(ii) The difference between $I^{(\mathrm{p})}_{\mathrm{r,\,Conv(II)}}$ and $I^{(\mathrm{s})}_{\mathrm{r,\,Conv(II)}}$ is due to the boundary conditions, but it is not very pronounced now. In both cases the currents respond correctly to M_{E}.

(iii) The neutral friction deserves particular attention. We approximate the neutral drag coefficient by [11]

$$\nu = n \cdot m \cdot n_n \cdot \langle \sigma \cdot V \rangle = n \cdot m \cdot n_n \cdot (10^{-8}(Ti^{0.318})) \qquad (24)$$

with n_n the neutral density and T_i the ion temperature expressed in eV, the profiles of which are given in Fig. 2. The current contributions found are given in Fig. 5. Neutral friction therefore can contribute strongly to the current, and would become the dominant source when the actual neutral density were to be higher than the computed one.

As this is the complete model we can compare it with a real experiment as for example performed on TdeV [5]. The comparison is possible as TdeV and TEXTOR are machines of comparable dimensions using ohmic plasmas for biasing experiments and $I^*_{\mathrm{r,\,conv}}$ does not depend on the average density. However the comparison of $I_{\mathrm{r,n}}$ and $I_{\mathrm{r,\,Vis}}$ is much more delicate as they largely depend on the exact neutral density and ion temperature profiles.

In the following table we compare $\mathrm{d}I^*/\mathrm{d}M_{\mathrm{E}}$, the rate of change of I^* with M_{E} found in TdeV with the predictions of our modelling.

Current	$\mathrm{d}I^*/\mathrm{d}M_{\mathrm{E}}$
$I^*_{\mathrm{r,\,TdeV}}$	−5.4
$I^*_{\mathrm{r,Conv(I)}}$	0
$I^{*(\mathrm{p})}_{\mathrm{r,\,Conv(II)}}$	−1.6
$I^{*(\mathrm{s})}_{\mathrm{r,\,Conv(II)}}$	−2
$I^*_{\mathrm{r},n}$	−3
$I^*_{\mathrm{r,\,Vis}}$	0

One notes that the combination of $I_{\mathrm{r},n}$ and either $I^{*(\mathrm{p})}_{\mathrm{r,\,Conv(II)}}$ or $I^{*(\mathrm{s})}_{\mathrm{r,\,Conv(II)}}$ is comparable to the experimental value and that the tiny difference between the latter two currents makes it impossible to judge which type of boundary condition is the more realistic.

5.3. The poloidal dependence of the currents

Although Eqs. (6) and (7) offer a powerful tool to compute the radial current, it is also interesting to study the poloidal dependence of the current densities.

We will do this for the two major contributions, namely $I_{\mathrm{r},n}$ and $I_{\mathrm{r,\,Conv(II)}}$. For the latter we will only consider the (s) boundary conditions as there is very little difference between the two cases when viscosity is included in the parallel momentum equation.

5.3.1. $I_{\mathrm{r},n}$

When we look at Eq. (9) and the considered neutral density profile (Fig. 2), we see that the two integrals contribute only very close to the plates. The current density due to neutral friction is therefore highly localised.

The reason why $I_{\mathrm{r},n}$ responds to changes in M_{E} is twofold.

(i) The second integral in Eq. (9) is proportional to M_{E}. This effect is rather weak because the term is multiplied by Θ^2.

(ii) The first integral contains M. When M_{E} is zero the M profile is practically symmetric, going from −1 to +1 (Fig. 4). As a consequence, two current densities flow at the level of the plates which are almost equal in magnitude but have opposite sign. This results in a current that is near to zero. When on the other hand M_{E} is different from zero, the M profile shifts up ($M_{\mathrm{E}} < 0$) or down ($M_{\mathrm{E}} > 0$), due to the Bohm–Chodura boundary conditions. Because of this the current densities at the plates become unequal in magnitude. The result is that the first integral in Eq. (9) gives a non-zero current.

We can conclude that the Bohm–Chodura criterion is at the basis of $I_{\mathrm{r},n}$.

5.3.2. $I_{\mathrm{r,\,conv(II)}}$

This current contribution, given by Eq. (11), can be written as the sum of two current densities:

$$J^{\mathrm{main}}_{\mathrm{r,\,Conv(II)}} = \frac{1}{B_\theta}\frac{1}{\sqrt{g}}\frac{\partial}{\partial\theta}\left(R\cdot\overline{\overline{\mathbf{T}}}_{\theta,\phi}\right) = \frac{1}{r\Theta B_{\mathrm{o}}R_{\mathrm{o}}}\frac{\partial}{\partial\theta}(R\cdot mnV_\theta V_\phi), \qquad (25)$$

which is also present in a straight geometry, and

$$J^{\mathrm{curvature}}_{\mathrm{r,\,Conv(II)}} = \frac{1}{B_\theta}\frac{1}{\sqrt{g}}\overline{\overline{\mathbf{T}}}_{\theta,\phi}\frac{\partial R}{\partial\theta} = \frac{1}{r\Theta B_{\mathrm{o}}R_{\mathrm{o}}}mnV_\theta V_\phi\frac{\partial R}{\partial\theta}, \qquad (26)$$

which is due to the curvature of the flux surfaces.

Fig. 6 shows the related reduced current densities, defined in the same way as the dimensionless current (Eq. (21)).

We see that the curvature part is smaller and varies less than the main part, although it reaches about 50% of the main part at the right hand side of the domain. The steep increase of J^*_{main} is mainly due to the shape of the Mach profile.

When M_{E} changes to +0.4, the profiles (not shown here) are lowered, giving then rise to a negative total integral. The response of J^*_{main} to M_{E} is more pronounced than that of $J^*_{\mathrm{curvature}}$.

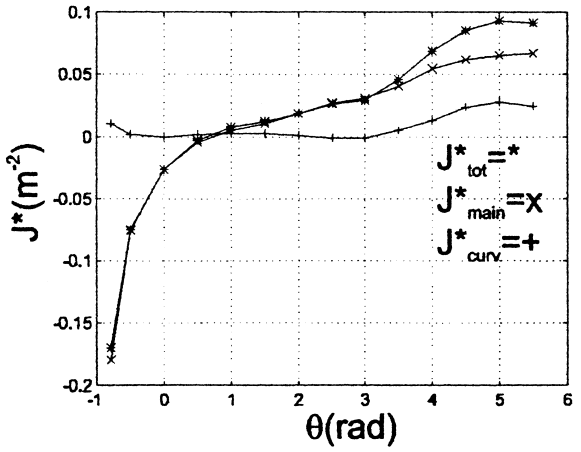

Fig. 6. The poloidal dependence of the different current densities contributing to $I_{\mathrm{rConv(II)}}$ when $M_E = -0.4$.

6. Conclusions

We have shown that the study of the radial current in the scrape-off layer is greatly aided by starting from the toroidal projection of the momentum equation, as in this case, provided all the curvature terms are retained, very compact expressions result, even when viscosity and neutral interaction is included. A detailed analysis of the relative contribution of convection, viscosity and neutral interaction in the radial current is then possible. The introduction of viscosity terms strictly weakens the impact of the modelling of the boundary conditions at the limiter or targets. Whereas the exact location where these are applied (the magnetic pre-sheath or the material boundary) have led in the past to strongly diverging results as discussed in Ref. [4], we now find that the experimentally observed dependence of the current on the radial electric field is retrieved under both conditions for the convectively driven current. It should be stressed that the influence of viscosity is mainly indirect, through its effect on the poloidal pressure profile via the continuity and parallel momentum equation. The direct effect, the viscosity driven radial current, is rather weak.

To explain the experimental results found on TdeV [5], our model shows that anomalous effects need not necessarily be invoked. Both convective and neutral interaction drive seem to be active, although detailed measurements are lacking to further evaluate the extent of the latter's role. In view of the strong dependence of the viscosity driven current on the ion temperature, a refinement of the model by including a temperature equation might still be in order.

We studied the Bohm–Chodura boundary conditions and further showed that the poloidal current densities can be studied and how they respond to the applied electric field.

References

[1] G.M. Staebler, Phys. Plasmas 1 (1994) 909.
[2] K. Itoh, S. Itoh, Plasma Phys. Fusion 38 (1996) 1.
[3] R. Weynants, G. Van Oost, Plasma Phys. Control. Fusion 35 (1993) B177.
[4] A. Chankin, P. Stangeby, Plasma Phys. Control. Fusion 38 (1996) 1879.
[5] J. Lachambre et al., Nucl. Fusion 34 (1994) 1431.
[6] V. Rozhansky, M. Tendler, Phys. Plasmas 1 (1994) 2711.
[7] M. Van Schoor, R. Weynants, Plasma Phys. Control. Fusion 44 (1998) 403.
[8] S. Braginskii, Rev. Plasma Phys. 1 (1965).
[9] M. Baelmans, PhD thesis, Institute für Plasmaphysik, Jül-2891 Series B, vol. 131, Plenum, New York, 1993.
[10] R. Chodura, Phys. Fluids 25 (1982) 1628.
[11] M. Harrison, Phys. of Plasma-Wall-Interactions in Controlled Fusion, NATO ASI Series B, vol. 131, Plenum, New York, 1986.